ADVANCED INTELLIGENT SYSTEMS
Open Access
www.advintellsyst.com

Inkjet Printing of Complex Soft Machines with Densely Integrated Electrostatic Actuators

*Samuel Schlatter, Giulio Grasso, Samuel Rosset, and Herbert Shea**

A multimaterial inkjet printing method for integrated soft multifunctional machines is reported, combining dense arrays of electrostatic actuators, multilayer electrical routing, and complex networks of microfluidic channels in one printing process. Most additive manufacturing methods for soft robots are developed for devices driven by external fluidic pressure sources and are not suited to fabricate soft electrically driven actuators. To integrate electrostatic zipping actuators and microfluidics in stretchable soft machines without any rigid components, inks for sacrificial layers, dielectric elastomers, and compliant electrodes are developed herein, along with a unified printing process to print multilayer structures. Printed 2.5D stacks are transformed into fully functional 3D soft machines by inflating thin elastomer channels. Two demonstrators are reported, each consisting of seven printed layers: a flexible peristaltic pump and a compliant slug drive, inspired by the locomotion of slugs. The peristaltic pump has six integrated actuators, whereas the slug drive has 28 integrated actuators, generating a travelling wave used to transport objects. These soft devices demonstrate how inkjet printing produces densely packed high-voltage actuators, including vias for electrical routing. Sensors and logic may be printed in the future to produce more complex autonomous soft machines.

1. Introduction

Soft machines consist of distributed and interconnected actuators, sensors, logic elements, and ideally a power supply, integrated in a stretchable body. Their intrinsic compliance makes them interesting for a wide array of applications, from soft robotics[1] to organs on a chip.[2] The field has seen rapid growth, in view of the versatility of soft machines,[3] their ability to replicate animal-like motion,[4–7] their intrinsic safety for human interactions,[1] resilience,[8–10] and the ability to use material compliance and elasticity as a means to both simplify control and add function.[11]

Given the highly integrated nature of complex soft machines, and the need for many different materials for functional and structural elements, additive manufacturing is an appealing method both to create soft machines with multiple independent actuators and to rapidly tailor dimensions, material properties, and device functions to different tasks.[12,13] As a fully printed soft machine requires no assembly, circuits and systems too complex for manual fabrication and assembly become possible. Printing has allowed complex soft structures with advanced materials,[14] but the focus to date has been mostly on pneumatic structures (i.e., printed chambers) and strain sensors for soft robot end effectors.[12,15] With a few exceptions such as the Octobot,[16] liquid-crystal artificial cilia,[17] or ionic electroactive polymers,[18–20] nearly all printed actuators are pneumatically driven fluidic elastomer actuator (FEAs) devices requiring external air pressure connections to inflate or deflate the bladders.[1,21] Fluidic actuation requires elastomers with well-defined channels but needs no electrical elements. In contrast, including electrically operated actuators embeds the electromechanical conversion into the device and reduces the number of external components. However, it adds important requirements, such as printing magnetic materials or metal coils for electromagnetic actuation, resistive tracks for Joule heating, or dielectrics with a high electrical breakdown, absence of pin holes, and the need for high thickness uniformity if electrostatic actuation is used. Actuators with embedded electrical actuation have been realized using printing processes, either partially printed in combination with additional fabrication methods or fully printed. The first category includes ionic electroactive polymers actuators, with printed polymer layers, but metallic electrodes deposited by other methods.[18,20] The second category includes hybrid pneumatic and shape memory polymer actuators with integrated Joule heating[22] or fully printed ionic microactuators.[19]

In this work, we use inkjet printing to produce complex soft machines with integrated electrostatic zipping actuators in a single process. We use a three-material printing process which

Dr. S. Schlatter, G. Grasso, Prof. H. Shea
Soft Transducers Laboratory (LMTS)
École polytechnique fédérale de Lausanne (EPFL)
Rue de la Maladière 71b, CH-2000 Neuchâtel, Switzerland
E-mail: herbert.shea@epfl.ch

Dr. S. Rosset
Biomimetics Laboratory
Auckland Bioengineering Institute
University of Auckland
70 Symonds Street, Auckland 1010, New Zealand

The ORCID identification number(s) for the author(s) of this article can be found under https://doi.org/10.1002/aisy.202000136.

DOI: 10.1002/aisy.202000136

enables complex interconnected structures comprising soft and stretchable elastomer parts, multilevel fluidic channels, and compliant electrodes. This makes it possible to fabricate entirely soft and stretchable functional devices, such as a peristaltic pump and a "slug" drive (**Figure 1**). One of the keys to developing compact and versatile soft machines is integrating the means of actuation in the structure of the device, instead of relying on external components, such as pumps or compressors.

Several paths to the untethered operation of soft fluidically driven devices without using compressors have been reported, including the use of chemical reactions to generate gas,[16] hydrolysis,[23] or electrohydrodynamic pumps.[24] Soft electrostatic actuators, such as dielectric elastomer actuators (DEAs), represent interesting alternatives for embedding electrically controlled actuation in a soft structure while providing large actuation pressure and a high response speed.[25] In their simplest configuration, they consist of a stack of three layers in which a soft elastomeric membrane is sandwiched between two compliant electrodes. The application of a high electric field (80–100 V μm^{-1}) leads to the compression of the elastomer membrane, which decreases in thickness and increases in area. DEAs can be used to move liquids and have been demonstrated as actuation means for soft pumps[26,27] or tunable liquid lenses.[28] A specific DEA-like configuration, electrostatic zipping devices, in which a dielectric fluid is introduced in the structure to form a pocket, is well suited to displacing liquids, obtaining a larger volume displacement compared with DEAs.[29] The fluid-filled dielectric layer deforms more easily than a pure elastomer layer, and the motion of liquid in the soft structure can be used for pumping or the generation of travelling waves. Although zipping actuation has been used for micro-electromechanical systems since the 1990s, its application to soft materials is more recent[30] and gained much traction in 2018, following a seminal article[29] in science from the Keplinger group, which demonstrated how zipping actuation can be applied to soft materials and liquid dielectrics to generate large displacements and forces. A higher performance with zipping geometries was achieved by Kellaris et al. with peano-HASEL devices[31,32] and by Taghavi et al. with electroribbon actuators.[33] The latter devices reach energy densities in the range of 10^5–10^6 J m^{-3} using inextensible polymers that can sustain very high electric fields. Zipping actuators with a liquid dielectric have been applied to different fields, such as microfluidics,[34] energy harvesting,[35] or haptic feedback,[36] thanks to their high displacement and force. Soft electrostatic zipping actuators are therefore interesting candidates to provide embedded electrically controlled deformation and liquid displacement for the actuation of soft machines, and developing a fabrication technique to seamlessly integrate these actuators into soft structures would enable the design of complex multi-degrees-of-freedom devices.

3D printing techniques are widely used to produce pneumatic-driven actuators for soft robots. Given the several millimetre thickness of most of these structures, bioprinters, extrusion, and direct ink write (DIW) printers have been used to directly obtain the desired chambers and channels, for instance, using the embedded 3D (EMB3D) approach.[15] However, for high-density electrostatic actuators, for which micrometre-thick layers of high-quality dielectric films with sub-millimetre printing of electrodes are required, layer-by-layer methods such as lamination,[37] blade casting,[38] dip coating,[39] spin coating,[40,41]

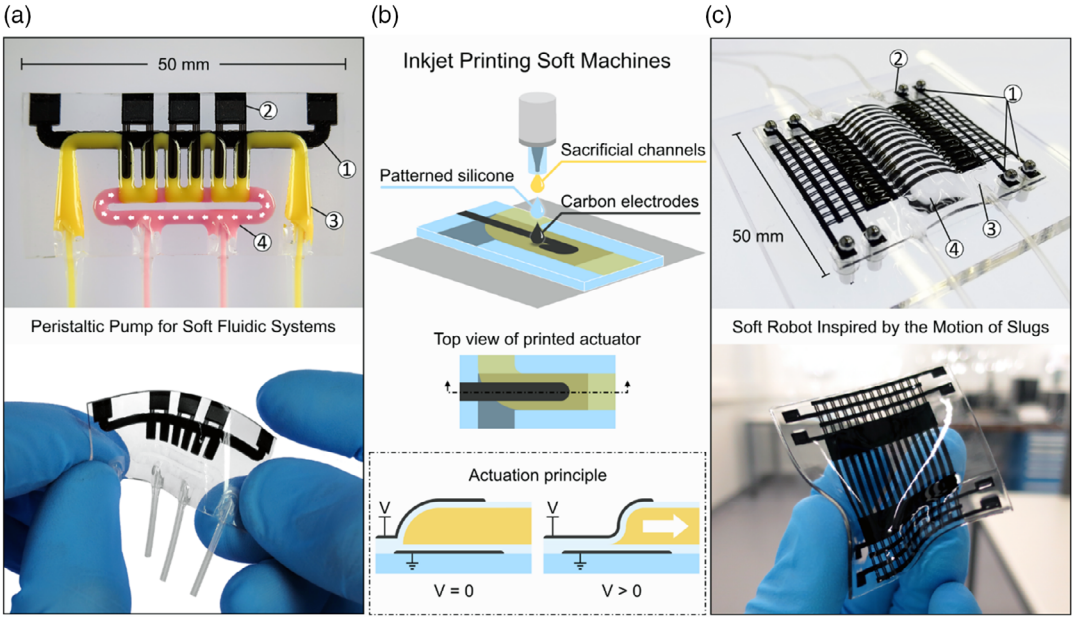

Figure 1. Complex soft machines fabricated by inkjet printing. a) A fluidic system with an integrated peristaltic pump and two separate fluidic networks. The channels have been filled with dyed fluids to make them visible. In operation the yellow channel contains a dielectric fluid and the pink channel contains the fluid to be pumped. ① Ground electrode, ② High-voltage electrodes, ③ dielectric channel, ④ aqueous channel. b) The stretchable soft machines are inkjet printed using multiple layers of electrode, silicone elastomer, and sacrificial material to create electrostatic zipping actuators and multilevel fluidic channels. c) The slug drive is a printed soft machine which mimics the travelling wave locomotion strategy of slugs, with 14 channels and 28 soft actuators. ① High-voltage phases (×3), ② ground electrode, ③ meandering dielectric channel, ④ liquid-filled cushion.

or pad printing[38,42] are preferred. In contrast to printed pneumatic actuators, printed electrostatic soft actuators not only depend on the mechanical properties of the printed layers, but also on their electrical properties, such as dielectric constant and elongation at break. To work with a reasonable actuation voltage (<5 kV), the dielectric layer thickness must be kept below 50 μm with good thickness uniformity to avoid dielectric breakdown in zones where the layer is locally thinner, and electrodes should be as thin as possible (typically <5 μm) and very compliant.[43] These requirements are beyond what can currently be achieved with 3D printing techniques, although there are some reports on 3D printed elastomeric membranes for DEAs. For example, Gonzales et al. used fused filament fabrication to print membranes from thermoplastic polyurethane that was subsequently prestretched to reduce their thickness,[44] and Rossiter et al. used a commercial Eden 350 V printer to print a photopolymer used as a dielectric membrane that was then mechanically biased out of plane to form a double-cone actuator.[45] For these two examples, the electrodes were manually applied due to the difficulty of depositing a very thin layer with a 3D printing process.

In this work, we use inkjet printing to create dense arrays of soft actuators in stretchable machines, combining the advantages of additive manufacturing with those of electrostatic actuation. Originally developed for printing text and images on paper, inkjet printing is now widely used to print functional materials and organic electronics. These materials are often flexible[46,47] but very rarely stretchable.[48] In theory, any substance can be patterned by inkjet printing, as long as it can be dissolved in a solvent or made into a liquid suspension (e.g., to print metals). The ability to dilute materials makes it possible to print very thin layers, often in the 100 nm range, of particular interest for lowering the voltage of electrostatic actuators and making it possible to deposit the very thin compliant electrodes required for soft electrostatic actuators. Inkjet printers with multiple print heads make it possible to print multilayer and multimaterial structures,[49] with higher spatial resolution than DIW methods. In practice, however, inkjet printing is a complex process in which the rheological properties of ink play a central role in determining the print quality. The challenges for inkjet (or more generally drop-on-demand) printing for integrated soft machines are 1) the development of printable inks to produce high-performance conductors, insulators, and sacrificial layers, 2) developing a unified process in which all materials are compatible with each other in terms of surface chemistry and solvents, 3) obtaining a 3D structure from a process that intrinsically generates thin 2.5D structures.

Although the potential of inkjet printing for the fabrication of DEAs has been identified by previous contributions, to date, the method has only been used as a tool to fabricate parts of the actuators (dielectric membranes or compliant electrodes). This is mainly due to the complexity of printing the different required materials together, as discussed in detail in Section 2.1. Regarding the printing of the dielectric membrane, we previously showed that silicone can be inkjet printed and produced micrometre-thick dielectric elastomer membranes.[50] The actuation performance of the printed films, to which compliant electrodes were added using pad printing, was comparable with the performance obtained on membranes that were created by casting. Regarding the printing of the compliant electrodes, inks for very soft stretchable electrodes have been developed. For example, Beachler et al. prepared the dispersion of multiwalled carbon nanotubes that were inkjet printed onto precast silicone membranes.[51] The electrodes were extremely thin (≈50 nm), yet maintained a high conductivity up to 25% stretch. Cabuk et al. developed a printable ink for DEA electrodes by diluting a commercial conductive carbon-loaded silicone.[52] As an example of multimaterial printing of dielectric elastomer transducers, Wilkinson et al. recently reported multilayer printed sensors using electrohydrodynamic printing for silicone layers and aerosol jet printing of a commercial graphene platelet ink for the electrodes.[53] Although Wilkinson et al. demonstrated the printing of the two main components (electrodes and membrane) of a dielectric elastomer transducer, the pressure sensor application used in the study is less demanding compared with actuators, as it doesn't require the layers to withstand high voltage or the electrodes to stretch more than a few percent. In addition, the elastomeric layer is a continuous layer and does not take advantage of the high-resolution patterning offered by the printing process. These examples show that the patterning of the primary components of a DEA by inkjet printing is possible. However, these materials have never been combined to print a complete actuator or a complex system integrating arrays of actuators, let alone fluidics. To produce more advanced soft machines, we must develop a compatible set of materials to produce complex multilayer structures.

In this work we report materials and methods to inkjet print complex soft machines. The stretchable materials include a carbon black-based electrode, a silicone-based dielectric, and a sacrificial polymer to define fluidic channels. We layer these materials to form multilayer DEAs, with embedded fluidic cavities and channels, as well as electrical interconnects. To illustrate the complexity and performance of soft systems printed with this process we demonstrate two devices, as shown in Figure 1. The first is a stretchable peristaltic pump, which uses integrated zipping actuators to pump aqueous liquids around a circuit. More complex fluidic systems may be fabricated by integrating additional pumps and valves. The second soft machine is the "slug drive," a conveyor inspired by the motion of slugs. The slug drive has 28 actuators integrated into a soft robot to mimic the travelling wave motion of the slug. It also shows how features printed in 2D can then be inflated to produce completely soft bodies. The two demonstrators show how inkjet printing may be used to build soft machines with densely integrated actuators and overlapping fluidic channels.

2. Results and Discussion

2.1. Inkjet-Printable Materials for Electrostatic Zipping Actuators

To inkjet print stretchable electrostatic zipping actuators, at least three materials are required: 1) a compliant electrode material, 2) an insulating elastomer with both structural and electrical properties, and 3) a sacrificial material that is used to produce fluidic channels. The materials must not only have the required properties to serve their function (e.g., conductivity or electrical

breakdown field), but must be compatible with multilayer printing. The latter constraint is a major challenge, as inks must be developed that not only provide high-performance functional materials when printed on several other materials, but must retain their properties despite solvent swelling from the layers printed above them.

While a range of conductive and insulating materials are commercially available as inks for drop-on-demand printers, they do not have the properties required for soft DEAs, principally very low stiffness (MPa range) and high elongation at break (>100%). Inkjet-printable conductive materials include dispersions of metals such silver and copper[54] and conductive polymers such as polyaniline (PANI), polypyrrole (PPY), and poly(3,4-ethylene diox-ythiophene) (PEDOT).[55] These materials are either brittle or too stiff to act as compliant electrodes for DEAs. Progress is being made on printable solutions of stretchable conductive polymers, but these still require solvents or chemical modification before use to tune viscosity and surface tension.[56] A number of groups have developed carbon-based inks for DEAs with good electrical properties,[51,57] but those materials have not been shown to be compatible with a fully printed approach, the electrodes were inkjet printed but not the dielectric ones, and there were no fluidic channels.

Given the paucity of suitable materials for inkjet-printed soft machines we have formulated a custom set of materials. Developing custom materials for inkjet-printed zipping elastomer devices is challenging because many factors must be considered. First the materials must be formulated to pass through the inkjet nozzle. In this work, a Jetlab 4 XL printer with 50 μm- or 80 μm-diameter piezoelectric nozzles is used. The piezoelectric nozzles can jet substances with a particle size less than 5% of the nozzle diameter and a viscosity between 0.5 and 40 cp. To achieve these fluid properties, a carrier solvent is used to put the powdered substances in suspension or to dilute soluble polymers. The volatility of this solvent must also be considered, as highly volatile solvents result in build-up and clogging of the nozzles, whereas solvents with a low volatility make it difficult to dry the printed layer.

Second, the interaction of inkjet-printed droplets with the underlying material must be considered. In inkjet printing, individual droplets are arranged on the previous layer to form lines and planes. These must be continuous and uniform to produce functional materials with predictable properties. However, low-viscosity droplets tend to coalesce. This occurs when the surface tension is high compared with the surface energy of the printing surface.[58] The surface tension may be reduced by adding surfactants and the energy of the printing surface may be increased with plasma or corona treatment. Another way to prevent droplets from coalescing is to rapidly evaporate the carrier solvent. This is a good approach to use for multilayer structures because it reduces the amount of time the solvent is present on the surface. If solvents are present for too long, they may redissolve materials printed earlier or swell the underlying polymers.[59] Swelling is undesirable because it causes the distortion of the printed layer and leads to a deformation of the printed geometry. Solvents with high volatility are therefore desirable, which conflict with the jetting requirements. In practice, a trade-off will be made between material build-up at the nozzle and the rate of drying of the printed layer. The plate and nozzle temperatures must thus be carefully selected. Rapid drying may amplify the coffee stain effect[60] and thus produce nonuniform layers. Extremely high temperatures may also cause the print head to heat up, resulting in erratic jetting or clogging of the nozzle.

Third, the materials must be converted from a liquid ink into a solid film. This may be accomplished by evaporating the solvents at ambient temperature or at elevated temperatures, by chemical curing, by photocuring, or by flash sintering. Problems may arise when the curing method for one material is incompatible with another. For example, heating an ink may cause the underlying materials to melt, degrade, or crack. Certain materials may also interfere with the curing process of others. For example, silicone addition curing can be poisoned by common materials such as vinyl plastics, chlorine-containing materials, certain epoxies, and vulcanized rubbers.[61] The interplay of different materials must therefore be carefully considered when printing multilayer and multimaterial structures.

In the remainder of this section, we describe the design of three inkjet-printable materials and associated printing methods that address the three aforementioned challenges to enable printing soft machines, as shown in Figure 1.

2.1.1. Thin Compliant Electrodes

Our optimized electrode mixture consists of 3 wt% carbon black powder, 26 wt% silicone polyglucoside dispersant, and a siloxane solvent. The dispersant is a nonionic surfactant consisting of 20% silicone polyglucoside in a cyclopentasiloxane solvent and helps put carbon black in suspension in the nonpolar siloxane solvent. The silicone polyglucoside behaves like a viscous gel once the solvents have evaporated, which helps to loosely bind carbon black together and prevent it from flaking off. The rheological properties of the electrode mixture are shown in **Table 1**. The mixture may be printed directly onto silicone without any pretreatment. The siloxane solvent penetrates into cured silicone, effectively increasing the surface energy of the silicone.

Figure 2a shows how the electrode mixture is patterned on silicone. A 50 μm nozzle is used to achieve high-resolution conductors and electrodes. On the Jetlab 4 XL system, the material may be patterned in one of the two modes: vector and raster. Vector mode is the continuous jetting of droplets while the nozzle follows a defined path and is used for long narrow electrical connections. Raster printing is the traditional

Table 1. Rheological properties of the solutions for compliant electrodes, dielectric elastomer, and sacrificial layer directly after preparation, measured at 25 °C. The storage modulus and loss modulus are given for an oscillation torque of 307 μN m, corresponding to a shear stress of ≈1 Pa. Additional details on the rheological properties, such as viscoelastic properties as a function of shear stress, can be found in Supporting Information.

Ink	Density [g ml^{-1}]	Surface tension [mN m^{-1}]	Viscosity [mPa s]	Storage modulus [mPa]	Loss modulus [mPa]
Compliant electrodes	0.82	16.19 ± 0.04	1.95 ± 0.06	10.3 ± 3.0	21.5 ± 0.7
Dielectric elastomer	0.83	16.19 ± 0.06	3.67 ± 0.19	17.6 ± 1.2	38.4 ± 3.7
Sacrificial layer	0.79	23.17 ± 0.15	2.77 ± 0.22	12.6 ± 0.6	28.3 ± 0.8

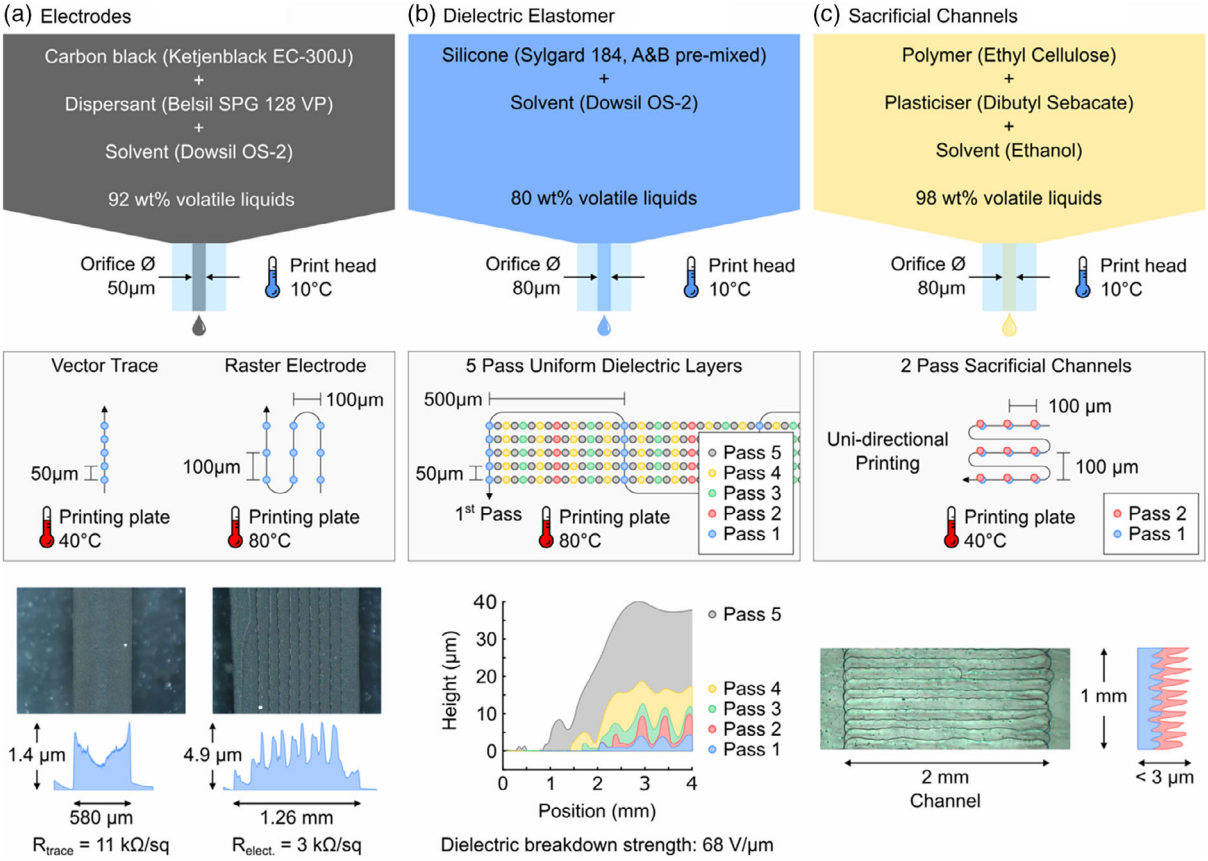

Figure 2. Materials developed for inkjet-printed multilayer soft machines. a) Carbon-based electrode material. b) Silicone-based dielectric material. c) Ethyl cellulose-based sacrificial material for printing channels. The first row shows the chemical make-up of materials. The second row shows how the materials are patterned. The last row shows the height profile of the printed materials.

drop-on-demand mode, where the nozzle scans the surface and deposits drops where needed. It is used to print large-area electrodes from a bitmap file. The printing plate is heated to accelerate the evaporation of the solvent. The print head is cooled with chilled water to 10 °C to reduce the rate of build-up and possible clogging of the nozzle. The vector traces and the raster electrodes are less than 5 µm thick after drying and show a sheet resistance of 11 and 3 kΩ sq^{-1}. With the printing plate at 40 °C, the line width of the vector trace is ≈580 µm. The line width can be reduced below 200 µm by increasing the printing plate temperature to 80 °C and droplet spacing to 100 µm (Figure S2, Supporting Information).

2.1.2. Dielectric Layers

Our printable silicone mixture consists of 20 wt% silicone elastomer (Sylgard 184, Dow), parts A and B, mixed as recommended by the manufacturer and dissolved in a siloxane solvent. The solvent is added for two reasons: although Sylgard 184 is a low-viscosity silicone (3500 cp), it is still 90 times more viscous than the viscosity limit specified by the printer manufacturer. The solvent reduces the viscosity of the mixture below 40 cp. Second, the solvent makes it possible to print sub-µm-thick dielectric layers, as 80% of the dielectric mixture is the solvent and evaporates on the printing plate. We opted to print layers ≈6 µm thick. The rheological properties of the dielectric mixture are shown in Table 1. The viscosity of the solution, given immediately following preparation in the table, exhibits no noticeable change over an 8 h period, even though the silicone base, crosslinker, and catalyst are mixed together. About 24 h postmixing, viscosity increases by 1 mPa s, with a further increase of 1 mPa s after 48 h. The time dependence of viscosity and viscoelastic properties of silicone ink are given in Supporting Information (Figure S7 and S8, Supporting Information).

Printing ink with a high solvent content is challenging when the substrate does not absorb the solvent in a spatially uniform manner. We developed a special printing procedure to obtain uniform silicone thickness when printing on a layer consisting of different materials (e.g., printing over cured silicone, electrode, and sacrificial regions). When the elastomer ink is printed on cured silicone, the solvent from the ink is readily absorbed by the underlying silicone. However, on other materials (electrode and sacrificial material) the solvent is absorbed more slowly. The difference in solvent absorption leads to solvent concentration gradients in the ink, causing undesired flows of the ink. The flows normally occur near material transitions producing thin and thick silicone regions after curing. The thin regions are mechanically and electrically weak and should be avoided. A method to deposit the material in five passes with varying

offsets was developed to reduce solvent flows. The principle behind the five-pass method is to deposit material gradually and allow the solvent to evaporate. Figure 2b shows how the droplets are arranged on the printing plate. On the first pass line spacing was set to 500 μm and an offset of 0 μm. On the second pass line spacing remains at 500 μm but the lines are offset by 250 μm to fill in the valleys of the first pass. On subsequent passes the line spacing and the offsets are halved. The droplet spacing is fixed at 50 μm for all passes. The first pass is most susceptible to solvent flows, but given that only a small proportion of the material has been deposited, it does not have a large impact on uniformity. Later passes deposit more material but are buffered by a viscous layer of silicone and are less impacted by the underlying materials.

Figure 2b (bottom) shows the cross section of the edge of a dielectric layer printed with the five-pass method. The uniformity of the printed dielectric layer improves as the number of passes increases. The result is a uniform dielectric layer with a thickness of ≈30 μm. The breakdown strength of the printed dielectric material was measured to be $68\,\mathrm{V\,\mu m^{-1}}$ (see Figure S1, Supporting Information).

2.1.3. Sacrificial Channels

In microfluidics, channels are generally fabricated by moulding against a silicon or polymer master and have a well-defined and roughly circular or rectangular cross section. Although some additive manufacturing techniques such as DIW can directly print channels with circular or rectangular cross sections, inkjet printing is not well suited for this. Inkjet-printed layers are extremely thin. Fabricating channels with a rectangular or circular cross section would require hundreds of passes and thus an overly long printing process.

A faster approach, which we developed here, is to print a thin sacrificial channel, a few μm thick, whose material acts as a separator, keeping subsequently printed silicone layers apart. Using sacrificial materials which do not adhere to silicone, it is possible to open the channels by inflating the channel after the entire device is printed. The process to open a thin sacrificial channel by peeling and inflating is shown in Figure S3, Supporting Information. The compliance of the soft machine allows these channels to be opened into a semi-circular cross section. The thin sacrificial channel approach is not only faster to print but produces channels which are faster to open, compared with having to dissolve the full channel height of sacrificial material.

The sacrificial mixture is a polymer (ethyl cellulose) dissolved in ethyl alcohol. Ethyl cellulose was chosen because it is readily soluble in ethanol, has good wetting properties on silicone, and a high volatility. In addition, it is not soluble in the silicone solvent that composes the elastomer and electrode inks, thus ensuring that the printed sacrificial layer remains unaffected when the subsequent layers are printed on top of it. A small amount of plasticizer, 10% of the weight of ethyl cellulose, is added to reduce cracking of the sacrificial layer.[62] The rheological properties of the sacrificial mixture are shown in Table 1.

Figure 2c shows how the sacrificial material is patterned on silicone. The sacrificial material was patterned unidirectionally and in two passes using the raster printing mode. Unidirectional printing ensures that each line has dried sufficiently before printing the next. Printing a second pass of the sacrificial channel ensures that there is full coverage. If a droplet misfires and leaves a hole it may not be possible to open the channel. The typical channel width is 2 mm, although channels down to 170 μm may be patterned in vector mode (Figure S2, Supporting Information).

Figure 2c shows a photograph and the profile of a printed sacrificial channel. The channel is 2 mm wide and passes vertically across the photograph. The profile of the channel is shown to the right of the photograph. The printed channel is less than 3 μm thick. This thin channel is transformed into a channel with a mm-scale cross section by peeling the layers apart, using air or fluid pressure. The absence of the vertical or steep channel wall also makes these types of channels better suited for zipping actuators (see the next section).

2.2. Design of Electrostatic Zipping Actuators

Figure 3 shows the design of a basic ink-jet-printed electrostatic zipping actuator. On the left of the figure are the top view, cross section, and exploded view of the actuator when printed (i.e., prior to filling the fluid channels). This actuator is fabricated by printing five layers, which form a capacitive structure, as shown in Figure 3b. After printing, the thin sacrificial channel is dissolved and replaced with a dielectric liquid. The process to open the channel is covered in more detail in Figure S3, Supporting Information. The schematic cross section of the filled but unactuated channel is shown in Figure 3d. When a voltage is applied the Maxwell stress is greatest where the electrodes are closest together. This point is shown in Figure 3d as the zipping origin. The electrodes are pulled together with a zip-like action, displacing the dielectric liquid toward the right-hand side of the channel. To ensure that zipping starts at one end of the channel, the high-voltage electrode is printed as a narrow track at the centre of the channel. If the high-voltage electrode had the same width as the channel and the ground electrode, zipping would occur from all sides, trapping dielectric fluid. The pressure generated by the actuator may be used to deform a channel or chamber to interact with other parts of the soft machine, as shown by the demonstrators later.

2.3. Inkjet-Printed Peristaltic Pump for Fluidic Systems

In this section inkjet printing is used to print a complex fluidic network with an integrated peristaltic pump. The ability to produce complex fluidic networks and accurately control the flow of liquids is essential in the fields of microfluidics and lab-on-a-chip devices (LOCs).[63,64] Microfluidic and LOCs typically require external pumps and pressure sources to actively pump liquids. Integrating actuators can reduce or eliminate the need for large and bulky external equipment.

The electrostatic zipping actuators presented in the previous section (section 2.2) can only pump dielectric fluids. Microfluidic and LOCs usually require pumping of aqueous liquids and electrolytes. We have therefore developed a coupled pumping scheme based on two independent fluidic circuits, one for the dielectric fluid and one for the liquid of interest for the LOC. A top view of the peristaltic pump is shown in **Figure 4**a.

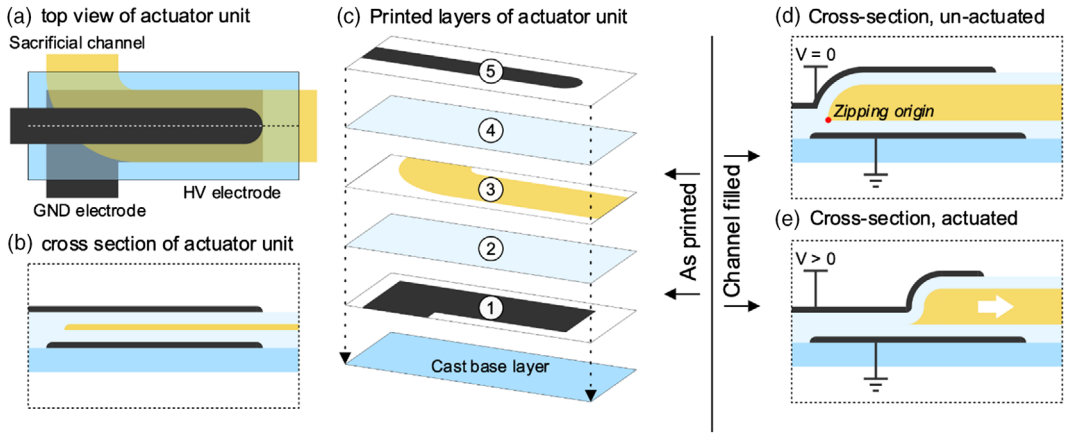

Figure 3. Design and working principle of inkjet-printed electrostatic zipping actuators. a) Top view of actuator. b) Cross section of actuator. c) Layered make-up of actuator. ① ground electrode, ② silicone dielectric layer, ③ sacrificial channel, ④ silicone dielectric layer, ⑤ high-voltage zipping electrode. d) Cross section of the zipping actuator when filled with a dielectric fluid. The zipping origin (red dot) shows where the electric field is initially highest and where the electrostatic zipping begins. e) Cross section of the zipping actuator when filled and actuated. Zipping begins on the left and displaces the dielectric liquid to the right.

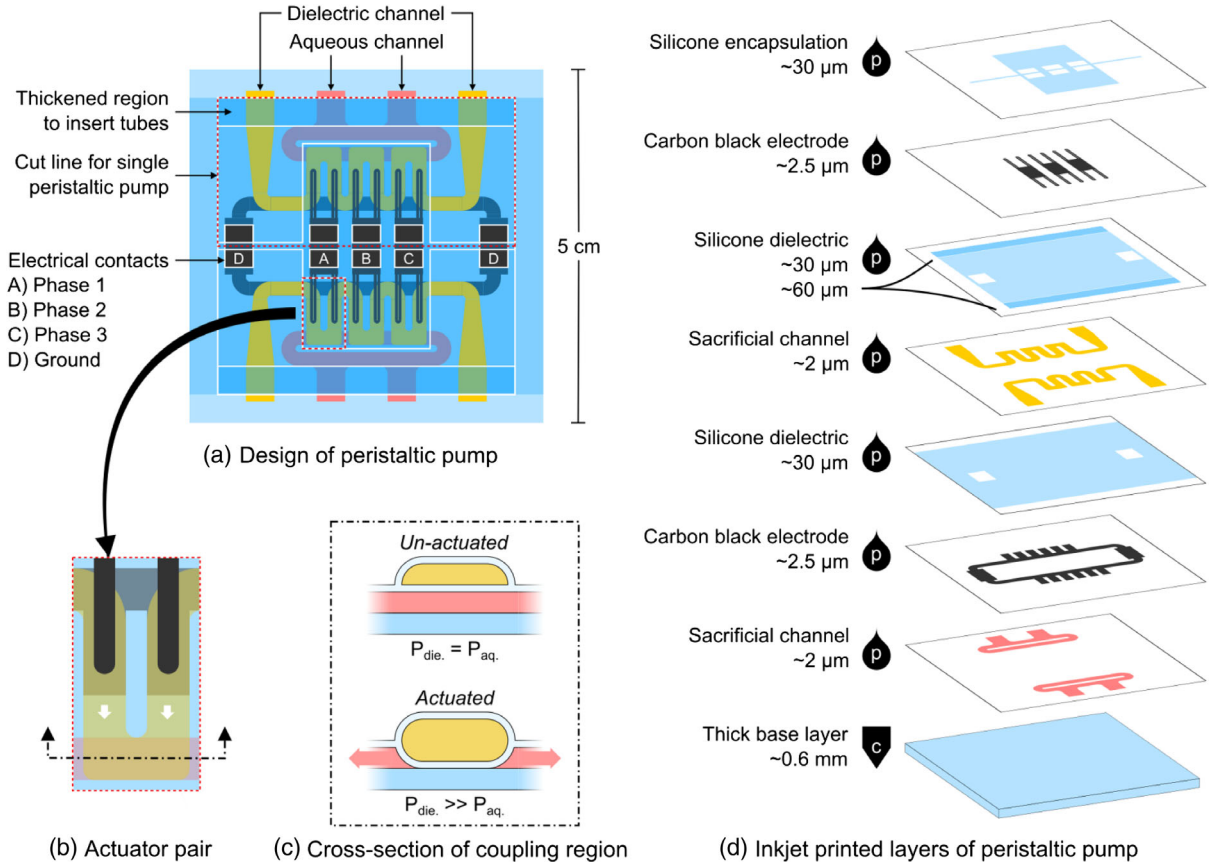

Figure 4. Design and function of the inkjet-printed peristaltic pump. a) Top view of the peristaltic pump. Two pumps are printed on a square 5 cm base layer. The pump consists of two independent fluid circuits, one containing a dielectric fluid (yellow) and the other an aqueous liquid (pink). The width of the fluidic channels is 2 mm. b) The aqueous liquid moves indirectly with a pair of electrostatic zipping actuators. c) Overlapping channels transfer the pressure from the dielectric channel to the aqueous channel. d) The layered structure of the peristaltic pump. The structure consists of a cast base layer and seven inkjet-printed layers. The approximate thickness of each of the layers is indicated.

Two pumps may be patterned on a 5 cm × 5 cm base layer. Each pump consists of two independent channel layers with a width of 2 mm, increasing to 4 mm at the edge of the device to enable connection with external tubing. The aqueous channel (pink) is printed first. The dielectric channel (yellow) is printed second. We used pairs of actuators, as shown in Figure 4b, to displace the dielectric fluid and deform the channel in the region where the channels overlap. When the pressure of the dielectric channel exceeds the pressure of the aqueous channel it causes the membrane to deflect and displace liquid in the aqueous channel (Figure 4c). Three actuator pairs have been patterned along the aqueous channel to produce a peristaltic pump capable of generating a net flow in the aqueous channel.

Figure 4d shows schematically how the peristaltic pump is fabricated. The pump consists of a thick base layer and seven printed layers. The thick base layer was prepared by casting a 0.6 mm-thick layer of silicone (Sylgard 184, Dow) on a sheet of glass coated with a polyvinylpyrrolidone release layer. Once cured, the 0.6 mm-thick layer of silicone was peeled off and divided into 5 cm squares. The squares were placed on a rigid glass plate, which provides a convenient way to handle and align the soft machine during fabrication. The printing process is not fully automated, with the silicone layers cured in an external oven, although it is possible to cure the silicone layers in situ on the printing plate, which can be heated up to 120 °C. In the interest of printing multiple samples in parallel, this was not implemented. The total printing time for a pair of peristaltic pumps is ≈4 h, excluding curing. The Jetlab 4 XL system is a research and development system with a single active nozzle. A machine for production with multinozzle printheads could produce devices more quickly.

The final step in pump fabrication is adding the fluid connections. The pumps are separated and trimmed to expose the channels on the edges. The protocol to attach the tubes and open the channels is shown in Figure S3, Supporting Information.

Figure 5a shows a photograph of the pump. The aqueous circuit is filled with deionized water, although any fluid compatible with silicone can be used. The dielectric channel is filled with a low-viscosity dielectric fluid. A pressure regulator is used to set the pressure of both channels to 25 mbar. Once the pressure is equalized, the channels are blocked with mechanical clamps to remove the pressure regulator from the circuit. On the figure, we have kept external tubing for the purpose of experimentation and characterization. In normal operation, the channels would be closed at the edge of the device, and the external tubing removed, as shown on Figure 5a with ⊗, thus not requiring any external fluidic connection to function.

We characterized the flow of the pump by forcing the pumped liquid through an external circuit and measured the flow with a flow meter (see Experimental section). This was achieved by keeping the external tubing for the aqueous circuit (pink) and connecting it to a flow meter. On the device, the aqueous channel was clamped between the two inlets (i.e., opposite overlap zone B) to force the flow in the external circuit and through the flow meter. A three-channel high-voltage power supply was used to control the actuators.[65] The power supply applies a square wave with an amplitude of 3.8 kV and a phase lag of 120° to produce the peristaltic pumping sequence.

Figure 5c shows the pumped volume versus time of the peristaltic pump. The pulse flow typical of peristaltic pumps is observed. The rate of pulsation increases with frequency and the amplitude of pulsation decreases with frequency. A linear trendline is fitted to the first 20 s of these curves to calculate the flow rate. The pump produces flow rates of 6, 6.6, 11.4, 9, and 13.8 μL min^{-1} at 0.2, 0.4, 0.6, 0.8, and 1.0 Hz, respectively. Due to the large fluidic impedance of the system, when external tubing to the flowmeter is added (about 600 mm of tubing) and to the low pressure of the dielectric fluid circuit that only provides a low restoring force and therefore long unzipping time, the mechanical bandwidth of the pump is limited to about 0.2 Hz. As shown in Figure 5c, the amplitude of each pumping stroke decreases with increasing frequency, which leads to a pumping flow rate that is not proportional to frequency. Optimization of the pump design would improve the performance, although the measured flow rate (13.8 μL min^{-1} at 1 Hz) is already comparable with other elastomeric pumps driven by DEAs[26,27] and is

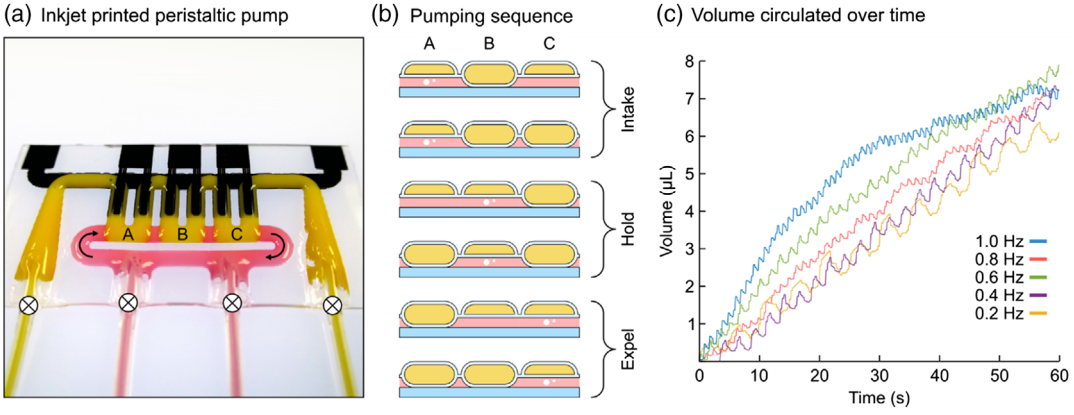

Figure 5. Printed stretchable peristaltic pump. a) A photograph of the peristaltic pump filled with coloured liquids for visibility. The regions where the channels overlap are denoted with 'A', 'B', and 'C'. Arrows show the direction of flow of the pink aqueous liquid. Note that the flow may be reversed by reversing the pumping sequence. Symbols (⊗) show where tubes would be cut and closed after filling the channel, to use the pump. For testing purposes, the external tubes are kept, which make it possible to adjust the pressure in each circuit. b) Peristaltic sequence used to pump the pink fluid by displacing the yellow dielectric fluid. c) Flow rate of the peristaltic pump through an external circuit, measured at five frequencies.

currently limited by the slow unzipping of the actuators, which limits the actuation frequency. The dynamics of zipping actuators with liquid dielectric is complex[66] and depends on many parameters, including the viscosity of the liquid, the geometry of the actuator, the impedance of the fluidic circuit, and the pressure in the two fluidic circuits.

The printed pump demonstrates that our multimaterial printing process enables the fabrication of flexible and stretchable functional devices without any rigid components. All parts of the pump are printed, including the actuation mechanism for the pump and two coupled fluidic circuits, leading to a device that only requires an external power supply. It highlights how inkjet printing can be used to realize multifunctional soft machines that are compact, integrated, and self-contained.

2.4. Inkjet-Printed Slug Drive for Soft Robots

The slug drive is a conveyor inspired by the locomotion of slugs and snails. Slugs and snails move by creating a travelling wave of deformation.[67] This unique form of locomotion allows them to travel over many different types of surfaces. Imitating the motion of invertebrate animals may give soft robots the ability to traverse difficult terrain.[68] The slug drive can also be used as a conveyor system if the actuators face upwards.

Our printed slug drive (**Figure 6**, **7** and **8**) replicates key aspects of the motion of slugs using a soft surface of parallel channels that are inflated and deflated in sequence to create a travelling wave. Because the system is made of elastomers, the spacing between the channels can change depending on which channels are inflated. The relative motion between channels and the changes in channel come in contact with the ground or an object enables locomotion or object transportation (Figure S4, Supporting Information).

The slug drive consists of a series of parallel channels, with a zipping actuator at each end. By activating the two actuators at the ends of a channel, the dielectric fluid is displaced, roughly doubling the volume in the central part of the channel, thus inflating it. To allow the channels to move freely, we pattern a

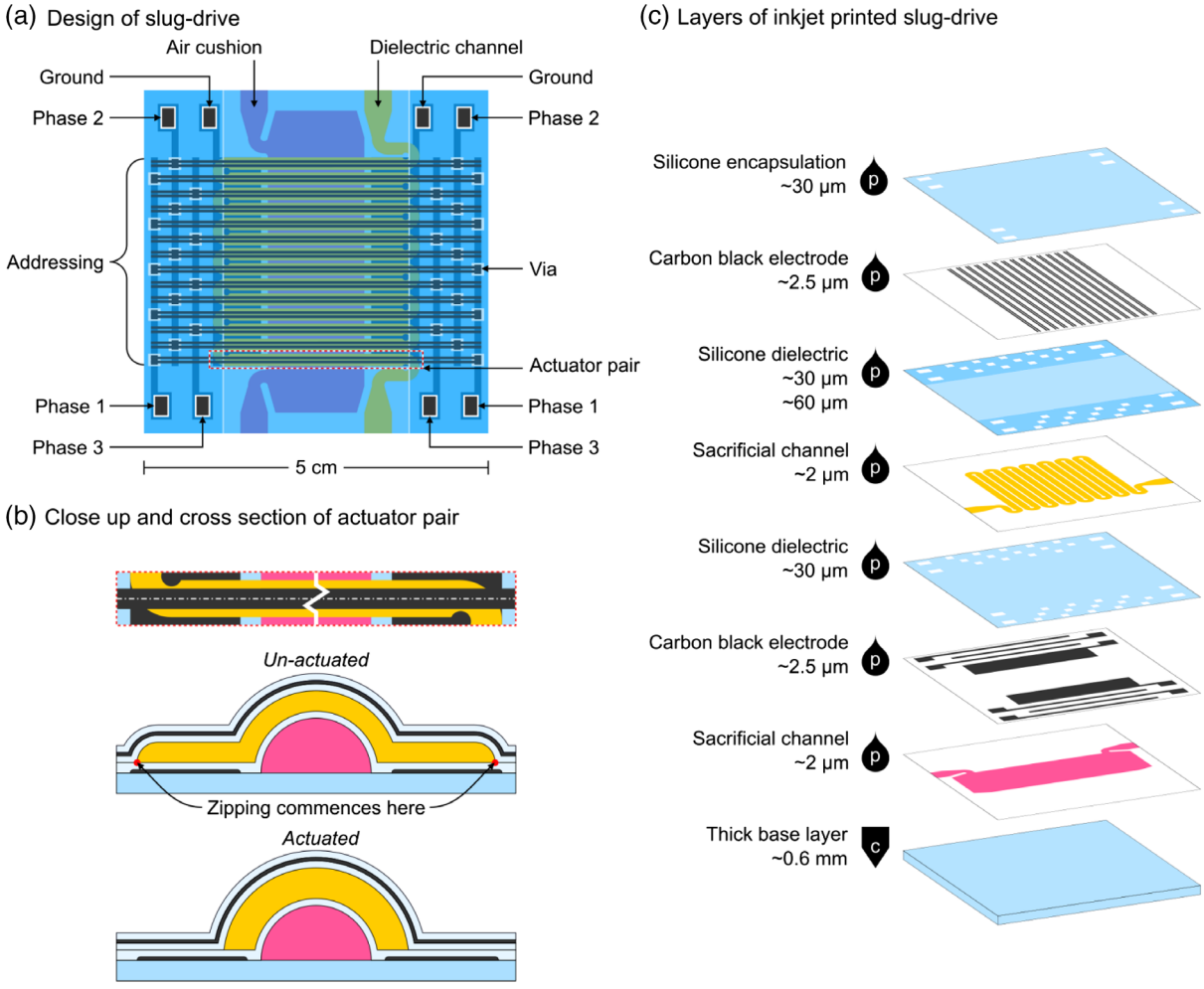

Figure 6. Design and actuation principle of the slug drive. a) Top view of a complete 14-channel slug drive. The lowest of the 14 parallel channels is highlighted with a dashed red line. b) Top view of one channel, and cross-section views showing how the dielectric channel (yellow) deforms when voltage is applied. c) The slug drive consists of a cast base layer and seven inkjet-printed layers. The yellow layer is filled with dielectric fluid for the zipping actuators. The pink layer ("cushion") is filled with air or with deionised water to lift the channels above the base layer, allowing the channel to move both in plane and out of plane.

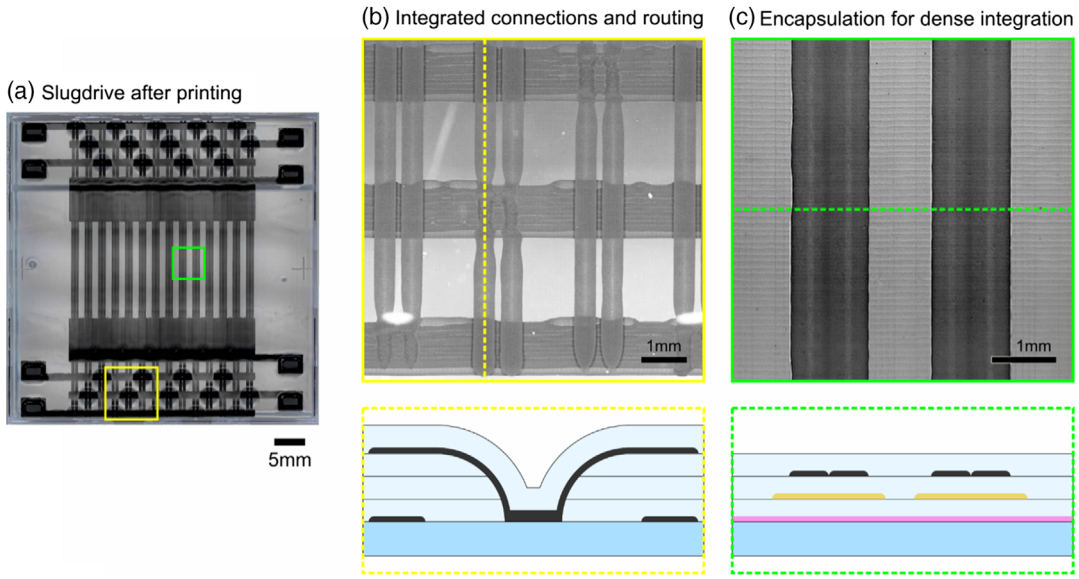

Figure 7. Inkjet-printed features enabling the dense integration of actuators. a) Microscope image of the slug drive as printed. b) Close-up and cross section of electrical vias. The ability to print holes enables dense multilayer routing. c) Close up and cross section of high-voltage zipping electrodes. The ability to print thin encapsulation layers enables closely spaced high-voltage conductors.

large cavity (the pink layer in Figure 6) under the central regions of the channel that can be filled with air or liquid, raising the channels above the base layer. The 28 actuators are grouped in 3 phases that are actuated sequentially (Figure S4, Supporting Information), leading to a travelling wave that can be used to move an object.

The parallel channels are produced initially as a single 1.8 mm-wide serpentine channel that changes direction 14 times, with a spacing between straight channels of 0.4 mm. A close up of one of the channels is shown in Figure 6b. The electrodes over the long middle part of the channel serve only to simplify electrical interconnects. The electrostatic zipping occurs only where the top electrodes (on the channels) overlap with the two larger lower electrodes, which are at ground potential.

Printed interconnects link the 14 top actuator electrodes to the three phases to reduce the number of external electrical connections. Power buses run along the edges of the device on the lower electrode level, with vias used to connect the top electrodes to the correct phase (easily seen in Figure 7a). Although power buses have been added on both sides of the device, only one side needs to be connected, thanks to the top electrodes extending over the whole width of the device. Consequently, the 28 actuators only require 4 external electrical connections. The vias are formed by leaving 1.6 mm square holes in the printed dielectric layers. The edges of the holes are not perfectly vertical. The dielectric layer around holes is tapered and takes ≈2 mm to reach full thickness (Figure 7b and Figure S6, Supporting Information, for height profile). For this reason the power buses were spaced by 2 mm. If this distance is not respected the dielectric layer between the power buses and the high-voltage zipping electrodes may be less than the designed 30 μm and thus lead to premature breakdown.

The ability to print multilayer structures makes it possible to print encapsulation layers (Figure 7c), which allows for densely integrated high-voltage actuators. High-voltage conductors with a voltage difference of 3.5 kV would typically have to be spaced by at least 3.5 mm to prevent breakdown in air. The encapsulation layer has a much higher breakdown strength than air, thus making it possible to reduce the spacing from 3.5 mm down to 50 μm. The encapsulation layers therefore provide a means to place high-voltage conductors and electrodes closer together, leading to more efficient integration.

The fabrication procedure for the slug drive is similar to the peristaltic pump. The slug drive consists of a thick (0.6 mm) silicone base layer prepared by casting and seven inkjet-printed layers. A single 14-channel slug drive is manufactured on a 5 cm × 5 cm square base layer. The inkjet-printed layers are printed in the order, as shown in Figure 6c, and it takes 4.5 h to print the slug drive on our single-nozzle printer.

The cushion layer is filled with deionized water and set to a pressure of ≈3 mbar. This pressure is sufficient to lift the channels off the base layer without kinking and blocking the dielectric channel. The channel is filled with a dielectric fluid and the pressure is set to 43 mbar. This pressure maximizes the channel cross section while permitting complete zipping. Spherical magnets are used to make electrical connections and fasten the slug drive to the testing platform. A three-phase high-voltage power supply provides the actuation waveform.[65]

A completed slug drive is shown in Figure 8a, with Figure 8b showing the channel deformation during actuation. The profile measurements in Figure 8d show the shape change as different phases are activated. The height of the actuated channel is ≈100 μm higher than the surrounding channels. The schematic diagram in Figure 8c shows how, in the actuated state, the channel is narrower and taller and applies tension to the neighbouring channels.

We validate the concept of the printed slug drive by conveying a small hexagonal plastic object (Nylon hex standoff, 15 mm

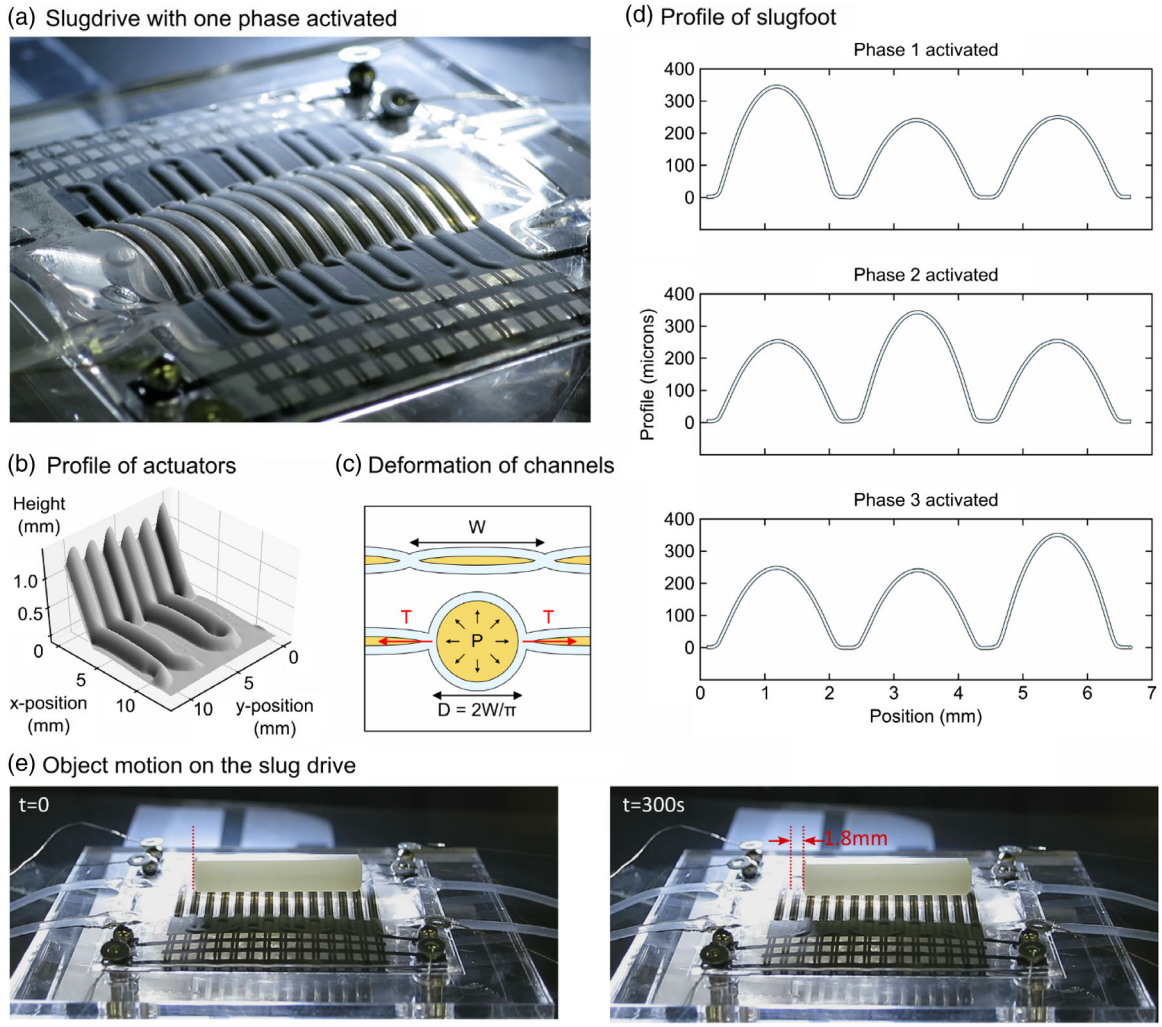

Figure 8. Photograph of the completed slug drive and profile measurements when actuated. a) Slug drive, with phase one active. b) The 3D surface scan of a corner of a slug drive with one phase active. c) Schematic illustration of the change of channel shape when actuated. The increase in pressure causes the channel to reduce in width and increase in height. The shape change applies tension to the neighbouring channels. d) Measured profile of the channels on the apex of the slug drive when different phases are activated. e) Conveying an object on the slug drive. A displacement of 1.83 mm is observed after 500 s (6.1 μm s^{-1}).

long). The area in contact with the slug drive is 3.2 mm × 15 mm, and the mass of the object is 0.26 g. It is placed on the apex of the slug drive, and a square wave with an amplitude of 3.5 kV and a phase offset of 120° between the three phases is applied to the device. At 0.1 Hz the object moves with a speed of 3.6 μm s^{-1}. At 0.2 Hz the speed of the object increases to 6.1 μm s^{-1}. The speed of the slug drive may be improved by optimizing the electrostatic zipping actuators to displace more volume. The speed of the object is dependent on the rate and magnitude of deformation. The rate of deformation is governed by the fluid properties and channel dimensions. A lower viscosity fluid and a shorter wider channel would therefore improve the performance of the slug drive. The magnitude of deformation is dependent on the actuation pressure, which can be increased using dielectric materials with a higher breakdown strength and a higher dielectric constant. We made a pneumatic proof-of-concept device slug drive to test different inflation conditions and achieved speeds up to 50 μm s^{-1} (Figure S5, Supporting Information). Changing materials and optimizing actuator geometry would allow for locomotion.

Our printed slug drive demonstrates how inkjet printing can produce densely packed high-voltage actuators, by patterning each layer, including the dielectric elastomer layer. This makes it possible to create vertical vias that enables multilevel electrical routing. Our demonstrator shows how a printed 2.5D stack can be transformed into a fully functional 3D soft machine by inflation of thin elastomer channels.

3. Conclusion

We developed a multimaterial inkjet printing method that allows the direct integration of soft actuators into multifunctional machines by fabricating electrical routing, electrostatic actuators,

crossing, and coupled microfluidic channels in one process. This enables one to take advantage of the high resolution of the inkjet printing process to produce dense arrays of actuators, while circumventing the limitation of the technique for the fabrication of 3D structures by fabricating inflatable structures.

DEAs and zipping devices are typically produced from sheet material. Consequently, most soft machines using electrostatic actuators have been planar devices with limited signal or fluidic routing and few actuators. The peristaltic pump and the slug drive show how inkjet printing may be used to densely integrate many actuators into stretchable machines. The slug drive has an area of 25 cm^2 and contains 28 integrated actuators, each with an area of 0.126 mm^2. Integrating many soft and high-voltage actuators into a small area was made possible by multimaterial and multilayer inkjet printing. Electrical and fluidic vias to route conductors or fluidic channels through different layers are straightforward to obtain when printing compared with other methods, as accurate holes in dielectric layers can be well defined as part of printing. This enables complex integrated electrical interconnections within the device and reduces the number contact pads, a key point for more complex machines with an even larger number of transducers.

To fabricate complex soft machines, we developed printable materials that are compatible with—and enable—a layering strategy. The materials include an electrode material based on carbon black, a dielectric material based on silicone, and a soluble sacrificial material based on ethyl cellulose to print channels. The electrode material and the dielectric material contain a nonpolar solvent, making it possible to layer the materials without any surface pretreatment. A novel method to produce channels in soft structures was presented, in which we print a 2 μm-thick sacrificial polymer between dielectric layers and then open the channels to 2 mm diameter by peeling and inflating.

The pump shows how electrostatic actuators may be used to control the flow of liquids. A similar approach may be used to create complex LOC devices with many pumps and valves. The soft machines presented here feature conductor traces and channels with a width of 0.5 and 2 mm. In the vector printing mode, our printer (JetLab4) can produce conductor traces and channels down to 180 μm wide (Figure S2, Supporting Information), approaching the scale of microfluidic circuits, but with a far higher density of actuators than in microfluidic chips. Aerosol jet printing would allow for even finer features.

The slug drive is a soft robot inspired by the motion of invertebrate animals. It demonstrates how inkjet printing may be used to produce soft robots with many densely integrated actuators. By further developing techniques to also print sensors and logic,[69,70] it will be possible to print smart soft machines.

4. Experimental Section

Electrode Ink: The electrode mixture was prepared by milling 5 g carbon black (Ketjenblack EC-300J, Akzo Nobel) with 45 g dispersant (Belsil SPG 128 VP, Wacker Chemie AG) in a three-roll mill (Exakt 50i, EXAKT Advanced Technologies GmbH). Here, the dispersant doubled as a grinding medium. The gap size was set to the minimum giving particles with a diameter below 10 μm. The resulting paste was combined with 20 g of silicone solvent (Dowsil OS-2 Silicone Cleaner and Surface Prep Solvent, Dow) and sonicated for 10 min. The mixture was rested for 10 min and decanted before use. The mixture was printed with a 50 μm nozzle (MJ-AT-01-50, MicroFab Technologies, Inc.). The printing parameters are shown in Figure 2a.

Silicone Ink: The silicone mixture was prepared in three steps. First, the base and initiator of silicone (Sylgard 184, Dow) were combined in a planetary mixer (Thinky ARE-250) in a 10:1 weight ratio—according to the manufacturer recommendation. The premixed silicone was added to the siloxane solvent (Dowsil OS-2 Silicone Cleaner and Surface Prep Solvent, Dow) in a 1:4 weight ratio and agitated to combine. The mixture was rested for 10 min and decanted before use. The dielectric mixture was deposited with an 80 μm nozzle (MJ-AT-01-80 from MicroFab Technologies, Inc.). The printing plate was set to 80 °C and the nozzle was cooled to 10 °C. The printing parameters are shown in Figure 2b. Printing was conducted in the raster mode, using five different bitmap images to accommodate the different line spacings and offsets. The printed layers were cured in an oven at 80 °C for 35 min. We measured the profile of the printed dielectric layers with an optical profilometer (Wyko NT1100, Veeco Instruments Inc.).

Sacrificial Ink: The sacrificial mixture was produced by dissolving ethyl cellulose (sigma Aldrich 200689 10 cp 48% ethoxyl) in ethyl alcohol in a 1:64 weight ratio. The plasticizer (Dibutyl Sebacate, Sigma Aldrich 84840 97%) was added to the mixture with a weight ratio of one part for nine parts of ethyl cellulose. We printed the sacrificial channels in raster mode with an 80 μm piezoelectric nozzle (MJ-AT-01-80, MicroFab Technologies Inc.). The printing plate temperature was set to 40 °C and the print head was cooled to 10 °C. A droplet and line spacing of 100 μm and a speed of 50 mm s^{-1} produced a sacrificial layer with good coverage and a thickness of about 2 μm. The printing parameters are shown in Figure 2c.

Rheological Properties: Surface tension measurements are carried out through the pendant drop method (OCA 25, Dataphysics). A disposable 1 mL syringe with a PTFE-coated dispensing tip (Nordson, gauge 25) was filled with the liquid under test. An automated piston acted on top of the syringe, enabling controlled dosing ($\leq$0.1 μL s^{-1}). A video of the falling droplet was captured (16 frames s^{-1}), and evaluation of surface tension was conducted using the last frame before the fall. Three droplets were analyzed for each liquid under test. Viscosity measurements were carried out with a hybrid rheometer (Discovery HR-2, TA Instruments) at 25 °C using 25 mm Peltier parallel plates with a gap of 50 μm and at a shear rate of 2500 s^{-1}. The data were sampled at 1 Hz for 1 min, and each ink formulation was tested six times. The measurement of the viscoelastic properties was carried out on the same setup as for viscosity. The storage and loss modulus were measured at different shear stress values by applying oscillatory motion of the plate (10 rad s^{-1}) with an increasing amplitude (0.01–10 Pa). A resolution of three points per decade was used for the silicone mixture and one point per decade for the two other inks, with each measurement repeated three times. To study the time evolution of the silicone mixture, viscosity and viscoelastic properties measurements were repeated every 2 h for the first 8 h following preparation and then after 24 and 48 h.

Fabrication and Testing of the Pump: The seven layers of the pump were printed using the parameters for ink, silicone, and sacrificial layer described earlier. Two pumps were printed in parallel on the same substrate and were separated with a sharp razor blade. External silicone tubes were connected to the channels, as shown in Figure S3, Supporting Information. We used 'T'-shaped connectors to connect an external flow sensor (flow unit L, Fluigent). The aqueous liquid was forced through the flow sensor by blocking the internal circuit with a magnetic clamp ('X' in Figure 5a). The aqueous circuit was filled with deionized water and the dielectric channel was filled with a low-viscosity dielectric fluid (Fluorinert electronic liquid FC-40, 3M). A pressure regulator was used to set the pressure of both channels to 25 mbar, before closing the channels with a magnetic clamp. The flow rate was measured for a voltage of 3.8 kV, applied with a multichannel high-voltage power supply (Peta-pico-Voltron).[65]

Printing the Slug Drive: The fabrication procedure for the slug drive was similar to the process for the peristaltic pump. The cushion layer was filled with deionized water at a pressure of $\approx$3 mbar. The dielectric channel was filled with a dielectric fluid (Fluorinert electronic liquid FC-40, 3M) at a

pressure of 43 mbar. Spherical magnets were used to make electrical connections and fasten the slug drive to the testing platform. A confocal microscope (3D Laser Scanning Confocal Microscope VK-X1100, Keyence AG) was used to measure channel deformation during actuation. A voltage of 3.5 kV was applied to each phase in sequence with a multichannel high-voltage power supply (Peta-pico-Voltron).

Supporting Information

Supporting Information is available from the Wiley Online Library or from the author.

Acknowledgements

This work was funded in part by the European Union's Horizon 2020 research and innovation program under the Marie Skłodowska-Curie grant agreement no 641822-MICACT via the Swiss State Secretariat for Education, Research, and Innovation and by the Swiss National Science Foundation, grant number 200020_184661.

Conflict of Interest

The authors declare no conflict of interest.

Keywords

dielectric elastomer actuators, hydraulically amplified electrostatic actuators, inkjet printing, soft machines, soft robotics, zipping actuators

Received: June 17, 2020
Revised: August 6, 2020
Published online:

[1] P. Polygerinos, N. Correll, S. A. Morin, B. Mosadegh, C. D. Onal, K. Petersen, M. Cianchetti, M. T. Tolley, R. F. Shepherd, *Adv. Eng. Mater.* **2017**, *19*, 1700016.
[2] H. J. Kim, D. Huh, G. Hamilton, D. E. Ingber, *Lab Chip* **2012**, *12*, 2165.
[3] D. Rus, M. T. Tolley, *Nature* **2015**, *521*, 467.
[4] C. Branyan, C. Fleming, J. Remaley, A. Kothari, K. Tumer, R. L. Hatton, Y. Mengüç, in *IEEE International Conference on Robotics and Biomimetics (ROBIO)*, IEEE, Macau **2017**, pp. 282–289.
[5] C. Jordi, S. Michel, E. Fink, *Bioinspir. Biomim.* **2010**, *5*, 026007.
[6] J. Shintake, V. Cacucciolo, H. Shea, D. Floreano, *Soft Robotics* **2018**, *5*, 466.
[7] C. Laschi, M. Cianchetti, B. Mazzolai, L. Margheri, M. Follador, P. Dario, *Adv. Robot.* **2012**, *26*, 709.
[8] R. F. Shepherd, A. A. Stokes, R. M. D. Nunes, G. M. Whitesides, *Adv. Mater.* **2013**, *25*, 6709.
[9] E. J. Markvicka, M. D. Bartlett, X. Huang, C. Majidi, *Nat. Mater.* **2018**, *17*, 618.
[10] E. Roels, S. Terryn, J. Brancart, R. Verhelle, G. Van Assche, B. Vanderborght, *Soft Robot.* **2020**, https://doi.org/10.1089/soro.2019.0081.
[11] J. Shintake, S. Rosset, B. Schubert, D. Floreano, H. Shea, *Adv. Mater.* **2016**, *28*, 205.
[12] A. Zolfagharian, A. Z. Kouzani, S. Y. Khoo, A. A. A. Moghadam, I. Gibson, A. Kaynak, *Sens. Actuators A: Phys.* **2016**, *250*, 258.
[13] T. J. Wallin, J. Pikul, R. F. Shepherd, *Nat. Rev. Mater.* **2018**, *3*, 84.
[14] R. L. Truby, J. A. Lewis, *Nature* **2016**, *540*, 371.
[15] R. L. Truby, M. Wehner, A. K. Grosskopf, D. M. Vogt, S. G. M. Uzel, R. J. Wood, J. A. Lewis, *Adv. Mater.* **2018**, *30*, 1706383.
[16] M. Wehner, R. L. Truby, D. J. Fitzgerald, B. Mosadegh, G. M. Whitesides, J. A. Lewis, R. J. Wood, *Nature* **2016**, *536*, 451.
[17] C. L. van Oosten, C. W. M. Bastiaansen, D. J. Broer, *Nat. Mater.* **2009**, *8*, 677.
[18] J. D. Carrico, N. W. Traeden, M. Aureli, K. K. Leang, *Smart Mater. Struct.* **2015**, *24*, 125021.
[19] M. Tyagi, G. M. Spinks, E. W. H. Jager, *Smart Mater. Struct.* **2020**, *29*, 085032.
[20] M. Tyagi, G. M. Spinks, E. W. H. Jager, *Soft Robot.* **2020**, https://doi.org/10.1089/soro.2019.0129.
[21] F. Ilievski, A. D. Mazzeo, R. F. Shepherd, X. Chen, G. M. Whitesides, *Angew. Chem. – Int. Ed>* **2011**, *50*, 1890.
[22] Y.-F. Zhang, N. Zhang, H. Hingorani, N. Ding, D. Wang, C. Yuan, B. Zhang, G. Gu, Q. Ge, *Adv. Funct. Mater.* **2019**, *29*, 1806698.
[23] T. Kitamori, A. Wada, H. Nabae, K. Suzumori, in *IEEE/RSJ International Conference on Intelligent Robots and Systems (IROS)*, IEEE, Daejeon **2016**, pp. 543–548.
[24] V. Cacucciolo, J. Shintake, Y. Kuwajima, S. Maeda, D. Floreano, H. Shea, *Nature* **2019**, *572*, 516.
[25] R. Pelrine, R. D. Kornbluh, Q. Pei, J. Joseph, *Science* **2000**, *287*, 836.
[26] S. Solano-Arana, F. Klug, H. Mößinger, F. Förster-Zügel, H. F. Schlaak, *Smart Mater. Struct.* **2018**, *27*, 074008.
[27] J. J. Loverich, I. Kanno, H. Kotera, *Lab Chip* **2006**, *6*, 1147.
[28] S. Shian, R. M. Diebold, D. R. Clarke, *Opt. Express* **2013**, *21*, 8669.
[29] E. Acome, S. K. Mitchell, T. G. Morrissey, M. B. Emmett, C. Benjamin, M. King, M. Radakovitz, C. Keplinger, *Science* **2018**, *359*, 61.
[30] L. Maffli, S. Rosset, H. R. Shea, *Smart Mater. Struct.* **2013**, *22*, 104013.
[31] N. Kellaris, V. G. Venkata, G. M. Smith, S. K. Mitchell, C. Keplinger, *Sci. Robot.* **2018**, *3*, eaar3276.
[32] N. Kellaris, V. G. Venkata, P. Rothemund, C. Keplinger, *Extreme Mech. Lett.* **2019**, *29*, 100449.
[33] M. Taghavi, T. Helps, J. Rossiter, *Sci. Robot.* **2018**, *3*, eaau9795.
[34] M. Sadeghi, H. Kim, K. Najafi, in *IEEE 23rd International Conference on Micro Electro Mechanical Systems (MEMS)*, IEEE, Daejeon **2010**, pp. 15–18.
[35] M. Duranti, M. Righi, R. Vertechy, M. Fontana, *Smart Mater. Struct.* **2017**, *26*, 115014.
[36] E. Leroy, R. Hinchet, H. Shea, *Adv. Mater.* **2020**, 2002564.
[37] S. K. Mitchell, X. Wang, E. Acome, T. Martin, K. Ly, N. Kellaris, V. G. Venkata, C. Keplinger, *Adv. Sci.* **2019**, *6*, 1900178.
[38] S. Rosset, O. A. Araromi, S. Schlatter, H. R. Shea, *J. Visualized Exp.* **2016**, *108*, e53423.
[39] F. Klug, S. Solano-Arana, N. J. Hoffmann, H. F. Schlaak, *Smart Mater. Struct.* **2019**, *28*, 104004.
[40] H. F. Schlaak, M. Jungmann, M. Matysek, P. Lotz, presented at *Smart Structures and Materials 2005: Electroactive Polymer Actuators and Devices (EAPAD)* (Ed: Y. Bar-Cohen), San Diego, CA, May **2005**.
[41] H. Zhao, A. M. Hussain, M. Duduta, D. M. Vogt, R. J. Wood, D. R. Clarke, *Advanced Functional Materials* **2018**, *28*, 1804328.
[42] A. Poulin, S. Rosset, H. R. Shea, *Appl. Phys. Lett.* **2015**, *107*, 244104.
[43] S. Rosset, H. R. Shea, *Appl. Phys. A: Mater. Sci. Process.* **2013**, *110*, 281.
[44] D. Gonzalez, B. Newell, J. Garcia, L. Noble, T. Mamer, in *Proc. of the ASME 2018 Conf. on Smart Materials, Adaptive Structures and Intelligent Systems*, American Society of Mechanical Engineers Digital Collection, San Antonio, TX **2018**, p. V002T02A006.
[45] J. Rossiter, P. Walters, B. Stoimenov, in *Electroactive Polymer Actuators and Devices*, SPIE, San Diego, CA **2009**, p. 72870H.
[46] K. D. Harris, A. L. Elias, H.-J. Chung, *J. Mater. Sci.* **2016**, *51*, 2771.
[47] S. Khan, L. Lorenzelli, R. S. Dahiya, *IEEE Sens. J.* **2015**, *15*, 3164.

[48] E. Bihar, T. Roberts, E. Ismailova, M. Saadaoui, M. Isik, A. Sanchez-Sanchez, D. Mecerreyes, T. Hervé, J. B. D. Graaf, G. G. Malliaras, *Adv. Mater. Technol.* **2017**, *2*, 1600251.
[49] M. A. Skylar-Scott, J. Mueller, C. W. Visser, J. A. Lewis, *Nature* **2019**, *575*, 330.
[50] D. Mccoul, S. Rosset, S. Schlatter, H. Shea, *Smart Mater. Struct.* **2017**, *26*, 125022.
[51] C. Baechler, S. Gardin, H. Abuhimd, G. Kovacs, *Smart Mater. Struct.* **2016**, *25*, 055009.
[52] O. Cabuk, M. Wegener, B. Gruber, S.-O. Seidel, J. Maas, in *Electroactive Polymer Actuators and Devices (EAPAD) XXII* (Eds: Y. Bar-Cohen, I. A. Anderson, H. R. Shea), SPIE, Bellingham, WA **2020**, p. 60.
[53] N. J. Wilkinson, R. W. Kay, R. A. Harris, *Adv. Mater. Technol.* **2020**, *5*, 2000148.
[54] N. C. Raut, K. Al-Shamery, *J. Mater. Chem. C* **2018**, *6*, 1618.
[55] G. Cummins, M. P. Y. Desmulliez, *Circuit World* **2012**, *38*, 193.
[56] R. Luo, H. Li, B. Du, S. Zhou, Y. Zhu, *Org. Electron.* **2020**, *76*, 105451.
[57] S. Reitelshöfer, M. Göttler, P. Schmidt, P. Treffer, M. Landgraf, J. Franke, presented at *Proc. of Electroactive Polymer Actuators and Devices (EAPAD)* (Eds. Y. Bar-Cohen, F. Vidal), Vol. *9798*, Las Vegas, Nevada, April **2016**.
[58] A. Soleimani-Gorgani, in *Printing on Polymers*, Elsevier, Amsterdam/New York **2016**, pp. 231–246.
[59] J. N. Lee, C. Park, G. M. Whitesides, *Anal. Chem.* **2003**, *75*, 6544.
[60] A. Friederich, J. R. Binder, W. Bauer, *J. Am. Ceram. Soc.* **2013**, *96*, 2093.
[61] J. G. Sommer, *Troubleshooting Rubber Problems*, Hanser Publishers, Cincinnati, OH **2013**.
[62] R. Hyppölä, I. Husson, F. Sundholm, *Int. J. Pharm.* **1996**, *133*, 161.
[63] K. Choi, A. H. C. Ng, R. Fobel, A. R. Wheeler, *Annu. Rev. Anal. Chem.* **2012**, *5*, 413.
[64] L. M. Fidalgo, S. J. Maerkl, *Lab chip* **2011**, *11*, 1612.
[65] S. Schlatter, P. Illenberger, S. Rosset, *HardwareX* **2018**, *4*, e00039.
[66] P. Rothemund, S. Kirkman, C. Keplinger, *Proc. Natl. Acad. Sci.* **2020**, *117*, 16207.
[67] M. W. Denny, *J. Exp. Biol.* **1981**, *91*, 195.
[68] M. Rogoz, K. Dradrach, C. Xuan, P. Wasylczyk, *Macromol. Rapid Commun.* **2019**, *40*, 1900279.
[69] M. Garrad, G. Soter, A. T. Conn, H. Hauser, J. Rossiter, *Sci. Robot.* **2019**, *4*, eaaw6060.
[70] K. E. Wilson, E.-F. M. Henke, G. A. Slipher, I. A. Anderson, *Extreme Mechanics Letters* **2016**, *9*, 188.